Classification of the EOS using the reconstructed CCSN GW high-frequency feature in real noise

First IGWN Symposium on CCSN GW Theory and Detection

Alejandro Casallas-Lagos[1] Marek Szczepańczyk [2] Javier M Antelis [3] Anthony Mezzacappa [4] R. Daniel Murphy [5] Claudia Moreno [6] & Michele Zanolin[7]

[1] University of Warsaw, Warsaw, Poland
[2] University of Warsaw, Warsaw, Poland
[3] University of Tennessee, Knoxville, USA
[4] University of Tennessee, Knoxville, USA
[5] Tecnologico de Monterrey, Monterrey, Mexico
[6] Universidad de Guadalajara, GDL, Mexico
[7] ERAU, Prescott, USA

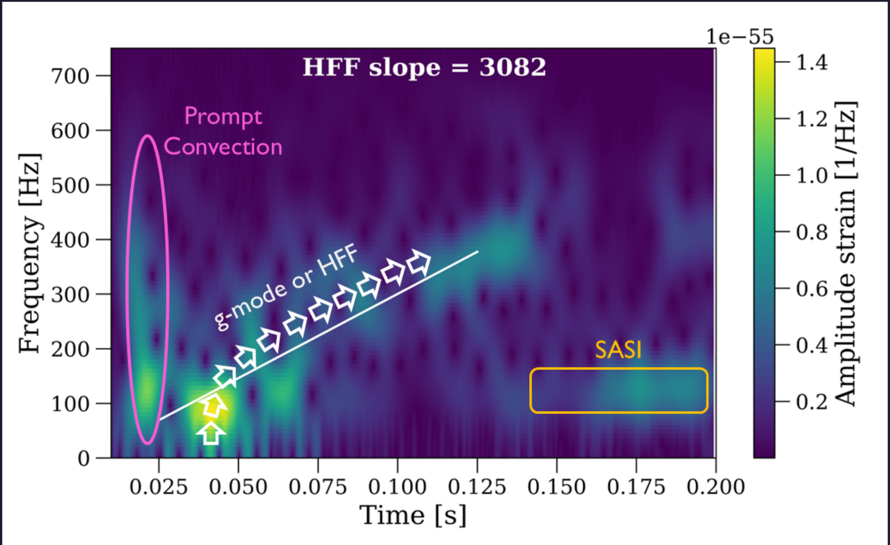

Figure 1: CCSN GW signatures.

Follow up of our previous papers:

1. Characterizing the temporal evolution of the high-frequency gravitational wave emission for a core collapse supernova with laser interferometric data: A neural network approach. https://doi.org/10.1103/PhysRevD.108.084027.
2. Dependence of the reconstructed core-collapse supernova gravitational wave high-frequency feature on the nuclear equation of state in real interferometric data. https://doi.org/10.1103/PhysRevD.110.083006.
3. Estimation of the High-Frequency Feature Slope in Gravitational Wave Signals from Core Collapse Supernovae Using Machine Learning. https://doi.org/10.3390/app15010065.

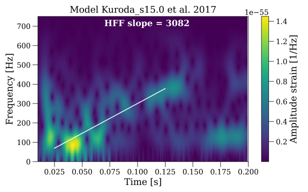

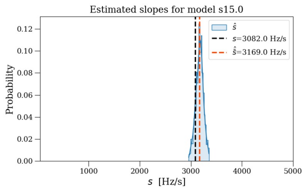

Figure 2: Previous results on PE for CCSN GWs in real LKV noise.

We extract GW signals from two-dimensional, axisymmetric CCSN simulations performed with the CHIMERA code. Five models were considered that employed five distinct EOS in the CCSN simulations: DD2, FSUGold, IUFSU, SFHo, and SFHx.

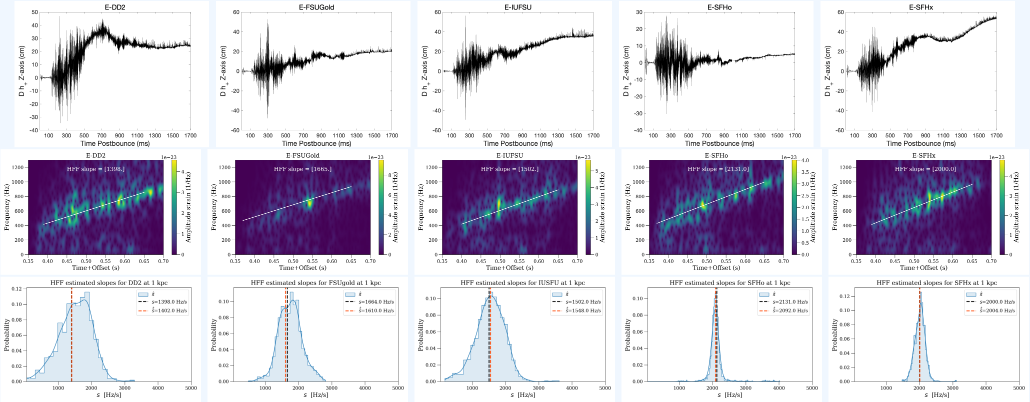

Figure 3: Top panel strains for each E-series model, middle panel spectrogram and bottom panel, in blue, the estimated slope of HFF. With red, dashed lines the estimated means of the HFF slope in the E-series spectrograms in LVK noise data (at 1 kpc). [Murphy et al. 2024]

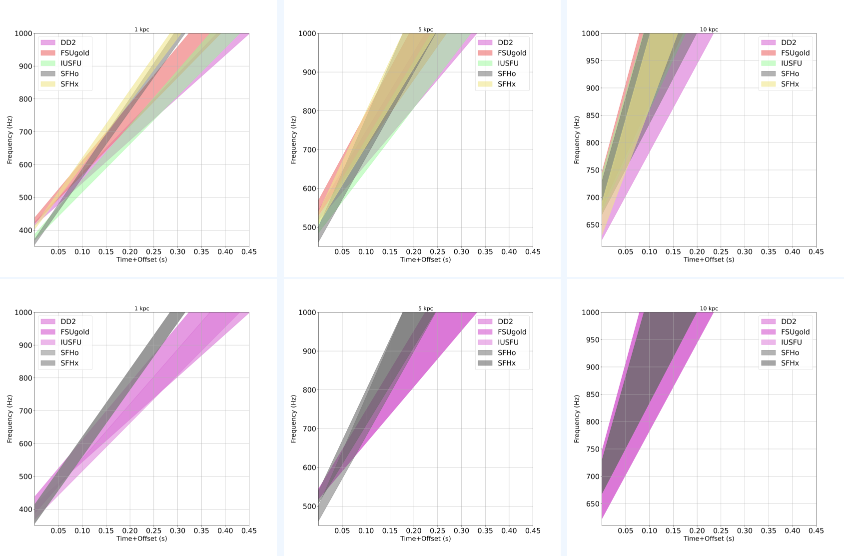

Figure 4: HFF slopes estimated including the range of variability of the HFF starting frequency across E-series models for detection distances of 1 kpc, 5 kpc, and 10 kpc [Murphy et al. 2024].

Clasiffication of the EOS according to the HFF slope

Is it possible to distinguish between the different EOS's using the estimated slope of the HFF in real interferometric LVK noise?

Time Window	TW1	TW1 (GPS time)	TW2	TW2 (GPS time)
Initial time	2019 – 11 – 03T00 : 00 : 01	1256774419	2019 – 11 – 17T00 : 00 : 01	1257465617
Final time	2019 – 11 – 10T23 : 59 : 59	1257984019	2019 – 11 – 24T23 : 59 : 59	1258675217

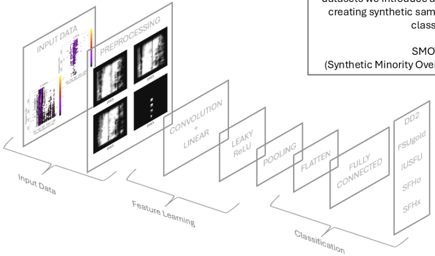

To address the class imbalance in TW1 and TW2 datasets we introduce a **SMOTE** technique by creating synthetic samples for the minority classes

SMOTE
(Synthetic Minority Oversampling Technique)

Figure 5: Overall structure of the CNN model implemented.

Results: TW1 EOS Classification

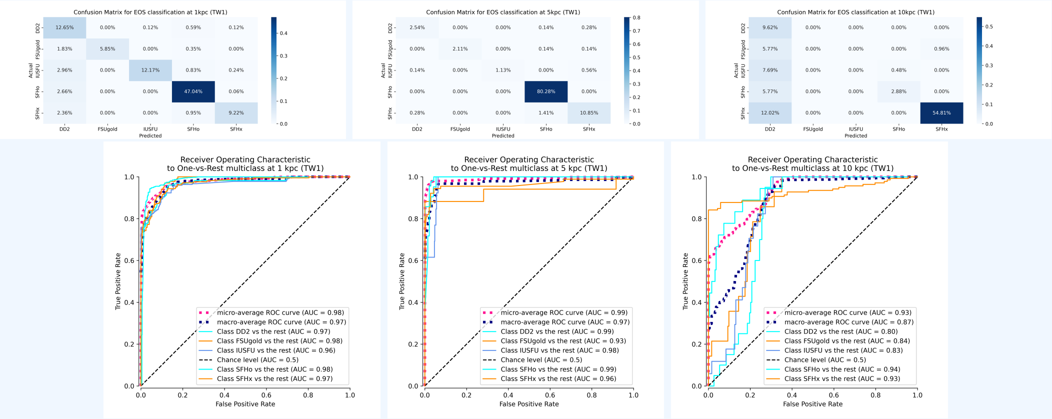

Figure 6: ROC curves and confusion matrices associated to the classification of the EOS at 1 Kpc, 5 Kpc, and 10 Kpc within the TW1. MICRO gives more weight to classes with more instances -MACRO It treats all classes equally, regardless of their frequency in the dataset.

Results: TW2 EOS Classification

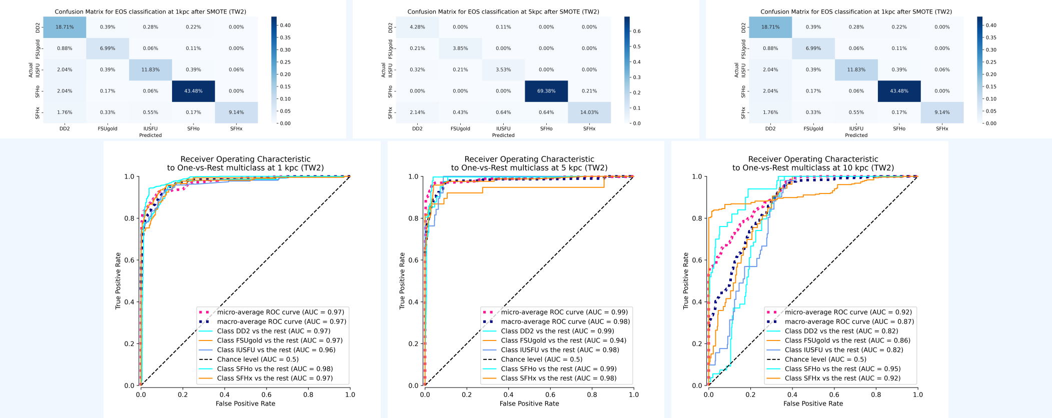

Figure 7: ROC curves and confusion matrices associated to the classification of the EOS at 1 Kpc, 5 Kpc, and 10 Kpc within the TW2.

RESULTS:

BEFORE SMOTE			
Metric	1 Kpc	5 Kpc	10 Kpc
Accuracy	0.88	0.85	0.87
Loss	0.32	0.43	0.31
Micro-Average OvR (AUC)	0.93	0.94	0.90
Macro-Average OvR (AUC)	0.91	0.94	0.83
AFTER SMOTE			
Metric	1 Kpc	5 Kpc	10 Kpc
Accuracy	0.89	0.87	0.89
Loss	0.34	0.36	0.37
Micro-Average OvR (AUC)	0.98	0.99	0.93
Macro-Average OvR (AUC)	0.97	0.97	0.87

BEFORE SMOTE			
Metric	1 Kpc	5 Kpc	10 Kpc
Accuracy	0.86	0.85	0.85
Loss	0.30	0.40	0.36
Micro-Average OvR (AUC)	0.94	0.93	0.89
Macro-Average OvR (AUC)	0.93	0.93	0.81
AFTER SMOTE			
Metric	1 Kpc	5 Kpc	10 Kpc
Accuracy	0.89	0.89	0.88
Loss	0.32	0.36	0.35
Micro-Average OvR (AUC)	0.97	0.99	0.92
Macro-Average OvR (AUC)	0.97	0.98	0.87

Figure 8: Accuracy, loss, micro-average OvR (AUC), and macro-average OvR (AUC) for the multi-classifier CNN before and after the application of the SMOTE technique on the datasets TW1 and TW2.

OvR (AUC)									
	1 kpc			**5 kpc**			**10 kpc**		
CLASS	TW1	TW2	TW1-TW2	TW1	TW2	TW1-TW2	TW1	TW2	TW1-TW2
DD2	0.97	0.97	0.97	0.99	0.99	0.97	0.80	0.82	0.85
FSUgold	0.98	0.97	0.96	0.93	0.94	0.96	0.84	0.86	0.89
IUSFU	0.96	0.96	0.97	0.98	0.98	0.97	0.83	0.82	0.85
SFHo	0.98	0.98	0.98	0.99	0.99	0.98	0.94	0.95	0.96
SFHx	0.97	0.97	0.97	0.96	0.98	0.973	0.93	0.92	0.94

Figure 9: ROC OvR AUC multiclass at Galactic distances of 1kpc, 5kpc, and 10kpc.

Conclusions:

1. Our analysis and implementation of this CNN architecture demonstrate the ability to precisely classify EOS based on the HFF estimated slope in LVK interferometric data.
2. This study advances the methodological framework for inferring EOS properties from CCSN GW signals:
   HFF slope estimation $\mapsto$ EOS HFF slope estimation $\mapsto$ EOS Classification$\mapsto$ Astro PE.
3. This progression, alongside the methodology for HFF slope estimation presented in our previous papers [Casallas-Lagos et al. 2023 and 2025], [Murphy et al. 2024], collectively enriches the suite of computational tools for contemporary CCSN GW parameter estimation, expanding avenues to investigate the fundamental nature of signatures encoded within these astrophysical signals.

Thank You!

Questions?